Dual-band all-dielectric chiral photonic crystal

Du, Lianlian; Liu, Yahong; Zhou, Xin; Tao, Liyun; Li, Meize; Ren, Huiling; Ji, Ruonan; Song, Kun; Zhao, Xiaopeng; Navarro-Cia, Miguel

DOI:
10.1088/1361-6463/ac4768

Dual-band all-dielectric chiral photonic crystal

Dual-band all-dielectric chiral photonic crystal

Lianlian Du[1], Yahong Liu[1*], Xin Zhou[2*], Liyun Tao[1], Meize Li[1], Huiling Ren[1], Ruonan Ji[1], Kun Song[1], Xiaopeng Zhao[1], Miguel Navarro-Cía[3,4*]

[1]School of Physical Science and Technology, Northwestern Polytechnical University, Xi'an 710129, People's Republic of China.

[2]The National Research Institute of Radio Spectrum Management, Xi'an 710061, People's Republic of China.

[3]School of Physics and Astronomy, University of Birmingham, Birmingham, B15 2TT, United Kingdom.

[4]Department of Electronic, Electrical and Systems Engineering, University of Birmingham, Birmingham B15 2TT, United Kingdom.

Corresponding author: Yahong Liu
E-mail:
[1]yhliu@nwpu.edu.cn
[2]zxbreeze@163.com
[3]m.navarro-cia@bham.ac.uk

Abstract

We present an all-dielectric chiral photonic crystal that guides the propagation of electromagnetic waves without backscattering for dual bands. The chiral photonic crystal unit cell is composed of four dielectric cylinders with increasing inner diameter clockwise or anticlockwise, which leads to chirality. It is demonstrated that the proposed chiral photonic crystal can generate dual band gaps in gigahertz frequency range and has two types of edge states, which is similar to topologically protected edge states. Hence, the interface formed by the proposed two-dimensional (2D) chiral photonic crystal can guide the propagation of electromagnetic waves without backscattering, and this complete propagation is immune to defects (position disorder or frequency disorder). To illustrate the applicability of the findings in communication systems, we report a

duplexer and a power divider based on the present all-dielectric chiral photonic crystal.

Key words: all-dielectric chiral photonic crystal, edge state, robust transmission, waveguide, duplexer, power divider

1 Introduction

The ability to control electromagnetic signals and energy has been one of the most important technological challenges. The introduction of topology brings this challenge into a new stage [1-3]. The topological insulator [4-6] is a quantum state with internal insulation and surface conductivity [7,8], which can exhibit topologically protected edge states. Recently, topological insulators have been extended to further areas of mechanics [9-14], acoustics [15-22], photonic [23-28] and electronics [29] with particular interests focusing on achieving topologically protected edge states that are immune to backscattering.

In recent years, photonic equivalents of condensed matter topological insulator have led to unprecedented opportunities in the control of electromagnetic waves [30-35], that has profound practical implications. Previously, topological edge states based on Quantum Hall effect were realized by applying external magnetic fields to break the time-reversal symmetry [36-40]. After that, the photonic crystals based on Quantum Spin Hall effect were proposed, which do not need to break the time-reversal symmetry [41-44]. In these photonic crystals, the topological nontrivial edge states are obtained by adjusting the parameters properly, and waveguides can be implemented by using the photonic crystals. For example, Gao presented a 2D all-dielectric photonic crystal, which confirms tunability and robustness of the topologically protected edge states [42]. Huang demonstrated topological protection of the edge states and reconfigurable topological one-way propagation, by inhomogeneously changing the ellipse orientation [44]. However, these systems only support the robust edge states along an interface between the topologically nontrivial and trivial photonic crystals, which is a stringent limitation for practical applications. More design flexibility and potential additional functionalities could be achieved if multiple types of robust edge states which is similar to topologically protected robust edge states are implemented in photonic systems.

Recently, chiral structures have gradually been investigated in photonic crystals, which provide a new method to control the transmission of electromagnetic waves. A

more robust property (chirality) is introduced into the photonic crystals [45-47]. As reported, most of these chiral structures are constructed by using air cavity structures or metal inclusions [48,49]. For example, Geng proposed a chiral 2D photonic crystal to realize the robust edge states transmission [48]. Orazbayev proposed a chiral protected optical waveguide, and verified its strong robustness and subwavelength transmission in experiments [49]. Although great progress has been made in the research of chiral structures, it is still a challenge for achieving multi-band all-dielectric chiral structure.

Unlike the previous reported chiral photonic crystal, in this work, we propose an all-dielectric dual-band chiral photonic crystal. The square unit cell of the all-dielectric chiral photonic crystal proposed here consists of four dielectric cylinders with different inner diameters. Depending on the rotational arrangement of the increasing inner diameter cylinders, the chiral photonic crystal displays two types of chirality. Both the chiral photonic crystals can generate dual-band gaps in gigahertz frequency range with associated edge states. We construct waveguides by using the present 2D structure. The numerical results show that the electromagnetic wave can propagate along the waveguide robustly without backscattering, and the transmission is immune to the defects (position disorders or frequency disorders). The proposed chiral photonic crystal can serve as a platform for basic on-chip components, illustrated here by a duplexer and a power divider.

2 Design and Analysis

Numerical simulations are performed by using a commercial simulation software High Frequency Structure Simulation Software (HFSS) based on three-dimensional finite element numerical analysis. In the simulation, all excitations are Hertzian-Dipole wave external source, and the red star indicates the external source. As shown in Figure 1(a), the proposed cylindrical dielectric is a high-dielectric constant ceramic with the relative permittivity of ε_r = 110 and tanδ = 0.0006. Such a ceramic can be obtained with a composition of CaO: SrO: Li_2O: Sm_2O_3:TiO_2 = 15: 1: 9 :12 :63 [50]. The outer diameter and height of the cylindrical dielectric are d = 8 mm and h = 7.47 mm, respectively. The lattice constant is a_1 = 13 mm. As the inner diameter of the cylindrical dielectric d_1 varies from 2.35 mm to 5.15 mm, the resonance varies from low frequency to high frequency as shown in Figure 1(b). We choose four cylindrical dielectrics corresponding to the resonance frequency of 3.6 GHz (f_1), 3.8 GHz (f_2), 4.2 GHz (f_3) and 4.6 GHz (f_4) to form a chiral subarray.

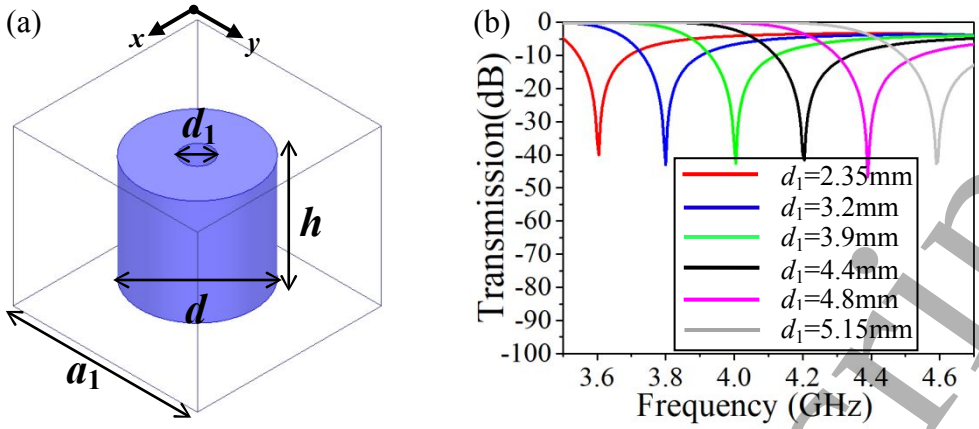

Figure 1. (a) Schematic view of the cylindrical dielectric cell. (b) Resonance curves for the various d_1.

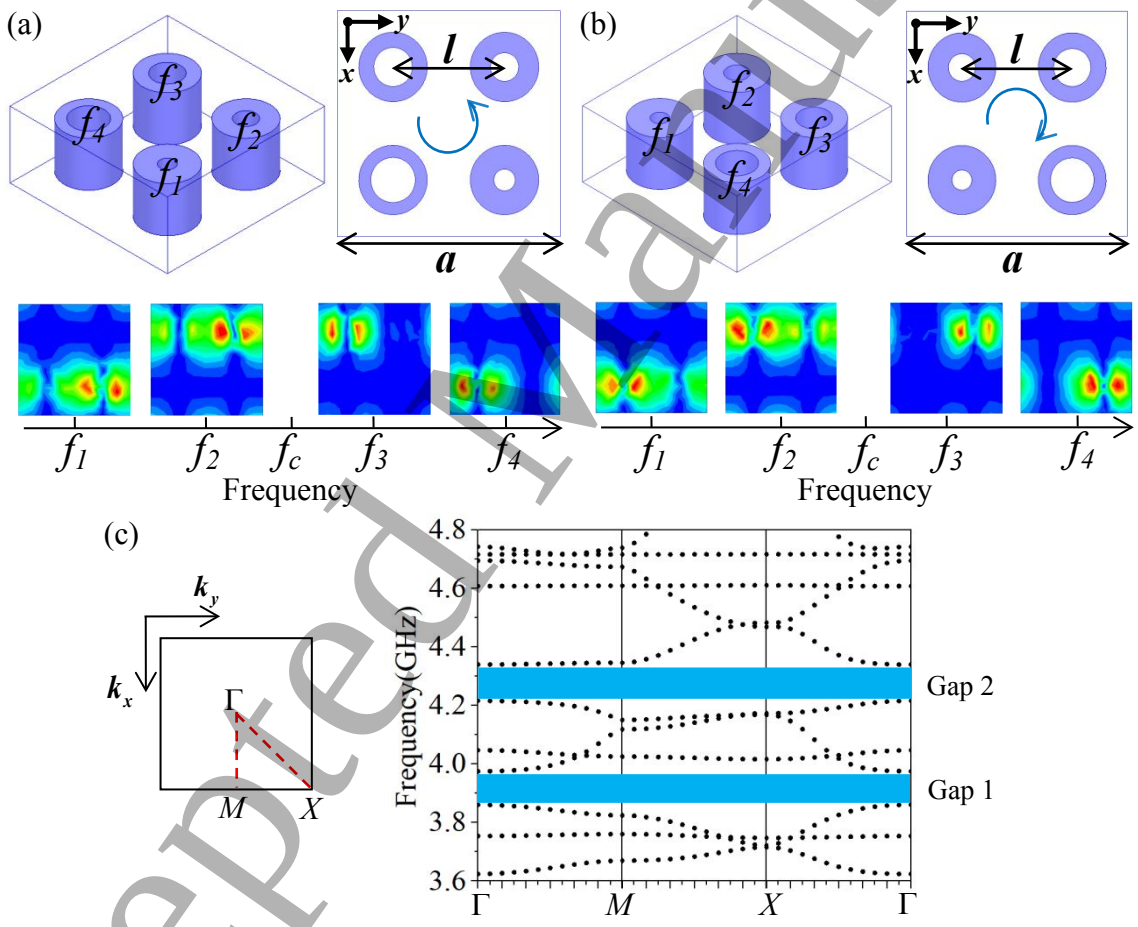

Figure 2. (a) Schematic diagram of the CCW chiral subarray. The lower panel is the electric field distribution of the CCW chiral subarray. (b) Schematic diagram of the CW chiral subarray. The lower panel is the electric field distribution of the CW chiral subarray. (c) Energy band diagram shared by the two kinds of chiral subarrays.

As shown in Figure 2, the lattice constant of the chiral subarray is a = 26 mm ($a \approx$

$\lambda_c/3$, λ_c is the wavelength corresponds to f_c = 4 GHz), which is twice than l= 13mm (l = a_1). As shown in Figure 2(a) and 2(b), the four cylindrical dielectrics (f_1, f_2, f_3, f_4) are arranged counterclockwise (CCW) or clockwise (CW) in a square lattice to form CCW chiral subarray or CW chiral subarray. CCW and CW chiral subarray show opposite chirality. The lower panel of Figure 2(a) and 2(b) show the electric field distributions of the two types of chiral subarrays, which indicates clearly that each resonant mode corresponds to one specific cylindrical dielectric cell. It is notable that the field energy is mainly localized on the resonator, but not between the resonators, which indicates that the coupling between the resonators is week. Since each cylindrical dielectric has the same eigen-frequency, these two kinds of chiral subarrays show the same dispersion relation. Figure 2(c) shows the energy band diagram of the two kinds of the chiral subarrays, where two band gaps are observed near the frequencies of 3.9 GHz and 4.3 GHz.

3 Edge states

3.1 Same chirality-induced edge states

Since the two kinds of chiral subarrays show the same dispersion, we investigate the edge states characteristics of the one-dimensional (1D) chain composed of the same chiral subarray. These edge states are demonstrated by using CCW chiral subarray as an example. We arrange the chiral subarray into 1D chain in x direction and y direction, respectively.

Firstly, we investigate the edge states arranged by the CCW chiral subarray along x direction. As shown in Figure 3(a), we construct a 1D chain composed of 10 CCW chiral subarrays arranged in x direction. Figure 3(b) shows the energy band diagram, where the red curves represent the edge states and the black curves represent the bulk modes. As $k_x = 0.5\pi/a$, four edge modes corresponding to four different frequencies are chosen from the dual band gaps, and the corresponding electric field distributions are presented in the right panel of Figure 3(b). It is shown that the electric field energy is mainly concentrated in the interfaces, indicating the existence of the edge states.

Secondly, we investigate 1D chain edge states arranged by the CCW chiral subarray along the y direction. As shown in Figure 4(a), we design a 1D chain consisting of 10 CCW chiral subarrays arranged in y direction. Figure 4(b) shows the energy band diagram of the corresponding 1D chain. We also focus on four edge modes at k_x=0.5π/a. The corresponding electric field distributions indicate that the energy is also mainly

concentrated in the interfaces.

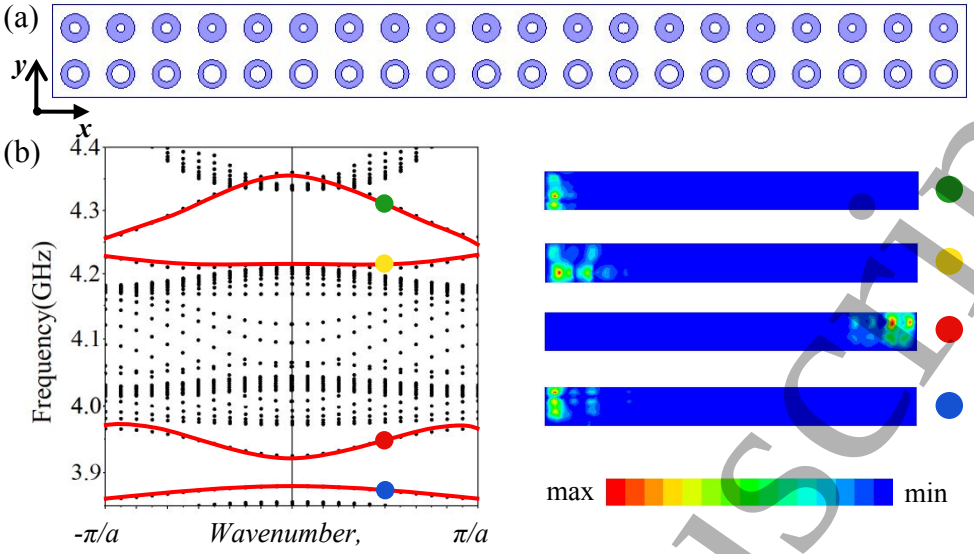

Figure 3. (a) 1D chain arranged by the CCW chiral subarray along the *x* direction. (b) Energy band diagram and the field distribution of the four edge modes.

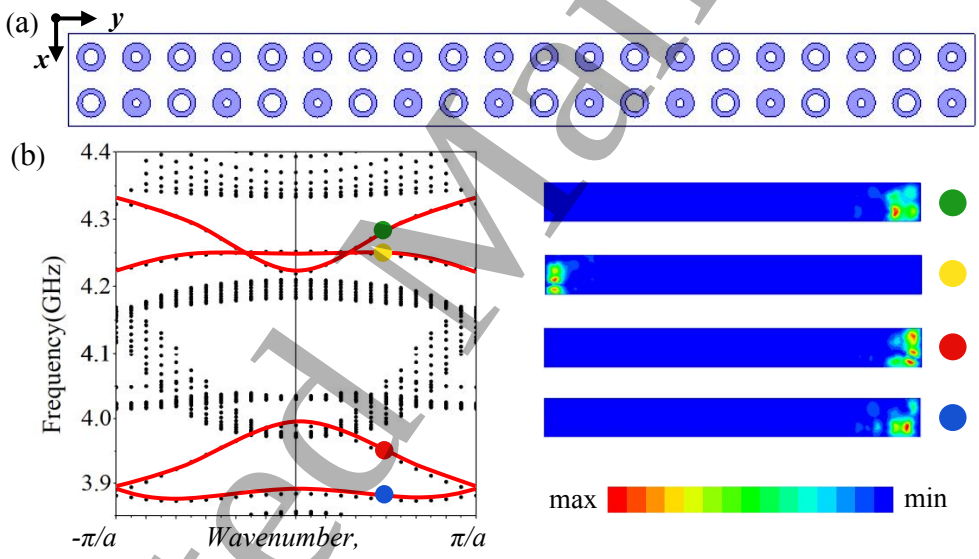

Figure 4. (a) 1D chain arranged by the CCW chiral subarray along the *y* direction. (b) Energy band diagram and the field distributions of the four edge modes.

3.2 Opposite chirality-induced edge states

In order to study the edge states at the linear chain constructed by subarrays with opposite chirality, we firstly analyze the resonant eigenmodes that are supported by the CW-CCW subarray formed by the two adjacent chiral subarrays as shown in Figure 5. Since this CW-CCW subarray (composed of eight cylindrical dielectrics) contains a new formed nonchiral subarray at the interface, it is expected to support additional eigenmodes. We focus on this new mode at resonance frequency of f_{a1}, where the

electric field distribution is presented in the lower panel of Figure 5(a). It is shown that the mode at f_{a1} is monopolar symmetric, and each cylindrical dielectric is oscillating in phase. Figure 5(b) presents the energy band diagram of the composite 1D chain composed of five CW chiral subarrays and five CCW chiral subarrays, where there is a new edge state near the frequency of f_{a1}. The lower panel of Figure 5(b) presents the simulated electric field distribution of the composite 1D chain, which shows that the energy is confined the interface of the nonchiral subarray. This property makes them good candidates as an elementary unit cell to create waveguide in an extended 2D structure.

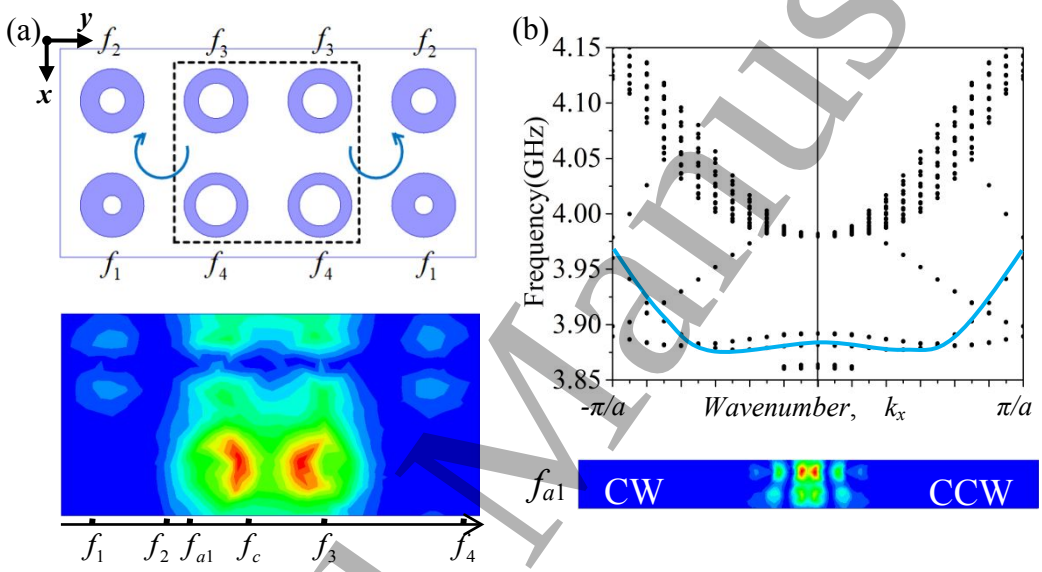

Figure 5. (a) CW-CCW subarray structure and the electric field distribution. The nonchiral subarray formed a new interface indicated with a black dashed line. (b) Energy band diagram of the composite 1D chain, and the electric field distribution at the frequency of f_{a1}.

In order to study the robustness of the edge state arising by the nonchiral subarray, we introduce a position disorder [51] and a frequency disorder in the 1D chain as shown in Figure 6(a). Monopolar mode f_{a1} has a good immunity to perturbation. To this end, we focus on the mode near the frequency of f_{a1}.

We first consider the edge state while introducing a position disorder. As shown in the left panel of Figure 6(a), the position disorder is obtained by moving the four cylindrical dielectrics of the nonchiral subarray by a distance R (randomly chosen R from 0 to $a/2$ in the xoy plane). The simulated electric field distribution near the frequency of f_{a1} is presented in Figure 6(b), which indicates that electric field energy is still localized in the interface. Next, we investigate the edge state while introducing a

frequency disorder. As presented in the right panel of Figure 6(a), we introduce the frequency disorder δf_c ($|\delta f_c| \leq 0.2$ GHz, $f_c = 4$ GHz) to the four cylindrical dielectric cells. The simulated electric field distribution near the frequency f_{a1} is shown in Figure 6(c). It can be seen that the electric field energy is still localized at the interface, indicating the proposed chiral subarray has a good robust edge state.

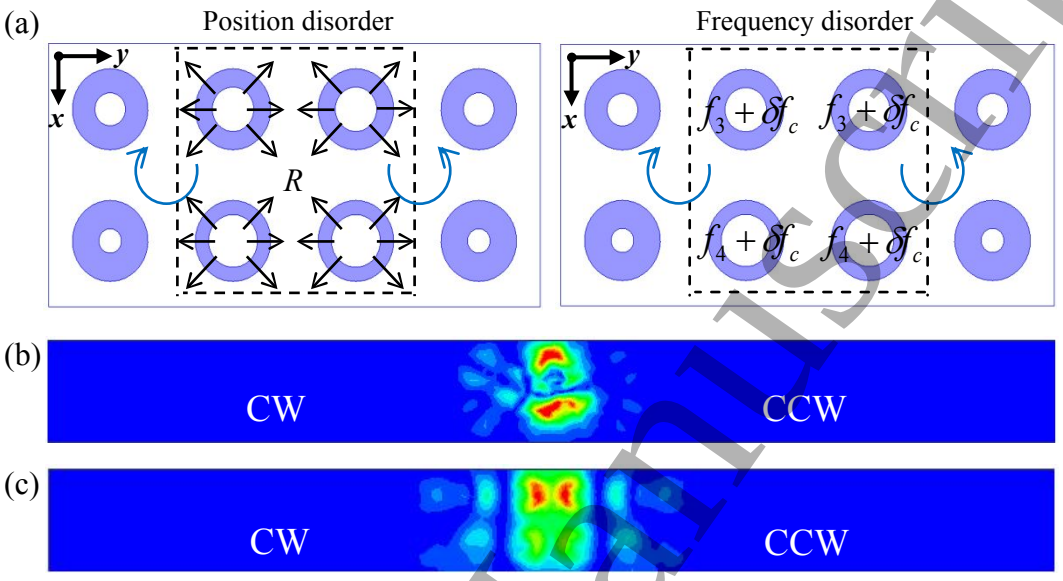

Figure 6. (a) Two kinds of perturbations: position disorder (left panel) and frequency disorder (right panel). Electric field distribution for (b) the position disorder and (c) the frequency disorder.

4 Chiral waveguides and robust transmission

4.1 Waveguides consisting of the CCW chiral subarrays

To better understand the transmission of electromagnetic waves in the edge states, we construct 2D square-waveguide by using the present chiral subarray. The CCW chiral subarray is firstly arranged into a 1D chain along the x direction, and then a 2D square-waveguide can be obtained by repeating the 1D chain along the y direction as shown in Figure 7(a). Figure 7(b) presents the electric field distribution of the 2D square-waveguide at 3.95 GHz within the first band gap, and Figure 7(c) presents the electric field distribution at 4.29 GHz within the second band gap. As demonstrated by Figure 7(b), electromagnetic waves propagate along the interface 12 and interface 13 with no obvious diffusion of backscattering in the first band gap. In contrast, as shown in Figure 7(c), the edge state in the second band gap propagates only along the interface 12. Figure 7(d) shows the transmission spectrums. Figure 7 shows that the transmission spectrums are in agreement with the simulated electric field distributions. Combined

with Figures 7(b) and 7(d), it can be seen that the electromagnetic wave can simultaneously transmit along the interface 12 and interface 13 at 3.95 GHz, where high transmissions are observed. Combined with Figures 7(c) and 7(d), the electromagnetic wave can only transmit along the interface 12 at 4.29 GHz, where a high transmission is also achieved.

The 2D square-waveguide shown in Figure 7(a) is formed by repeating a 1D chain along the *y* direction. It can be observed that the 1D chain is formed by a CCW chiral subarray along the *x* direction. Therefore, combined with the first edge mode shown in Figure 3(b), there is no edge state in the interface 13 at 4.29 GHz. Thus, electromagnetic waves cannot propagate along the interface 13. This feature enables us to envision frequency-dependent unidirectional waveguide.

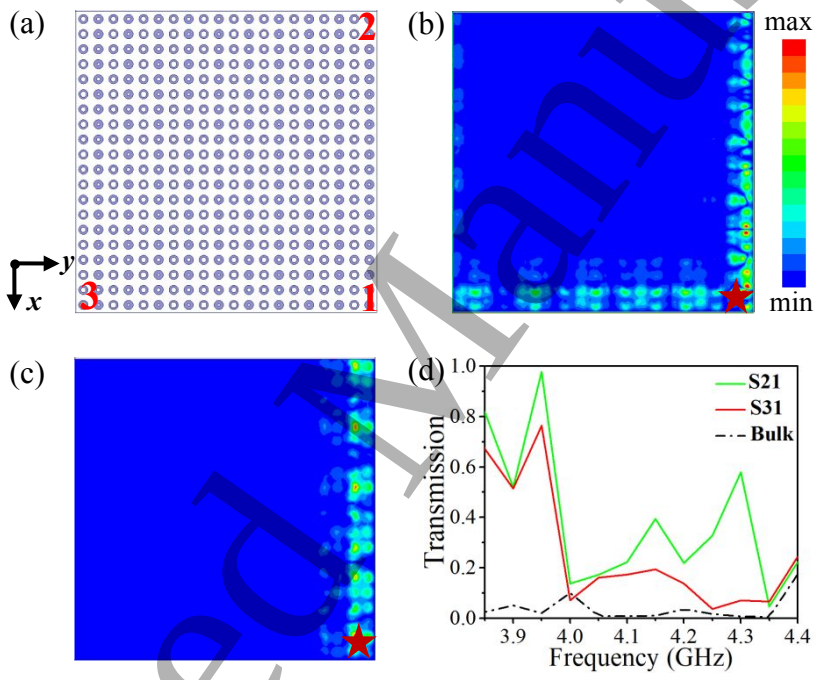

Figure 7. (a) 2D square-waveguide composed of the CCW chiral subarrays. Electric field distribution of the 2D square-waveguide at (b) 3.95 GHz and (c) 4.29 GHz. (d) Transmission spectrums of the 2D square-waveguide.

To demonstrate the robust propagation of the 2D structure as a waveguide, we construct a 2D *L*-shaped waveguide as shown in Figure 8(a). The Figure 8(b) shows the electric field distribution at the frequency of 4.29 GHz. The transmission spectrum presented in Figure 8(c) shows that a high transmission can be obtained around 4.29 GHz. The result is in agreement with the simulated electric field distributions. It is clear that electromagnetic waves can propagate along the *L* sharp corner without

backscattering, suggesting the potential robustness of the chiral waveguide. For the configuration of *L*-shaped waveguide, according to the edge modes shown in Figures 3(b) and 4(b), the *L*-shaped waveguide interface do not have edge states at the first bandgap of 3.95 GHz. Therefore, the electromagnetic waves cannot propagate along the *L* sharp corner at 3.95 GHz.

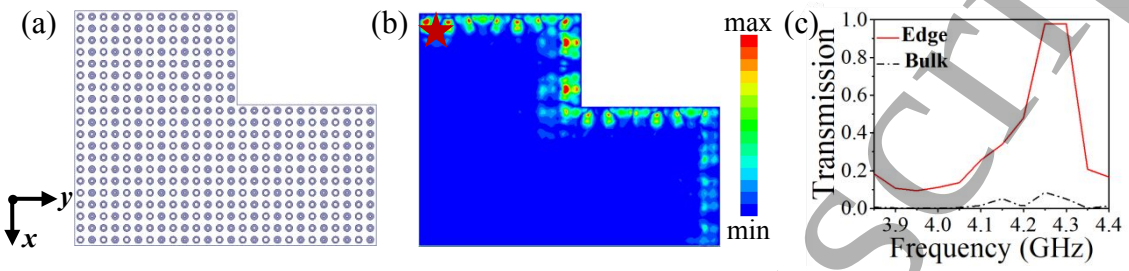

Figure 8. (a) *L*-shaped waveguide composed of the CCW chiral subarrays. (b) Electric field distribution at the frequency of 4.29 GHz. (c) Transmission spectrum of the *L*-shaped waveguide.

In order to further study the robustness of the edge states, we introduce a random position perturbation in the 2D waveguides. As shown in Figure 9, we move the four cylindrical dielectrics of a CCW chiral subarray by the distance *R* (randomly chosen *R* from 0 to *a*/4 in the *xoy* plane). As shown in the left panel of Figures 9(a)-(c), the red boxes indicate the location of the disturbance. The simulated electric field distributions are shown in the right panel of Figures 9(a)-(c). Figure 9(d) and 9(e) show the transmission spectrums, which are in agreement with the simulated electric field distributions. For the 2D square-waveguide with a position perturbation, the electromagnetic wave can transmit along the interface 12 and interface 13 around 3.95 GHz, where a high transmission can be achieved as shown in Figure 9(d). And around 4.29 GHz, the electromagnetic wave can only transmit along the interface 12, which also agrees with the transmission spectrum. As presented in Figure 9(e), a similar result can be obtained for the *L*-shaped waveguide. It can be seen that electromagnetic waves can still propagate along the interface, suggesting the robustness of the chiral waveguide.

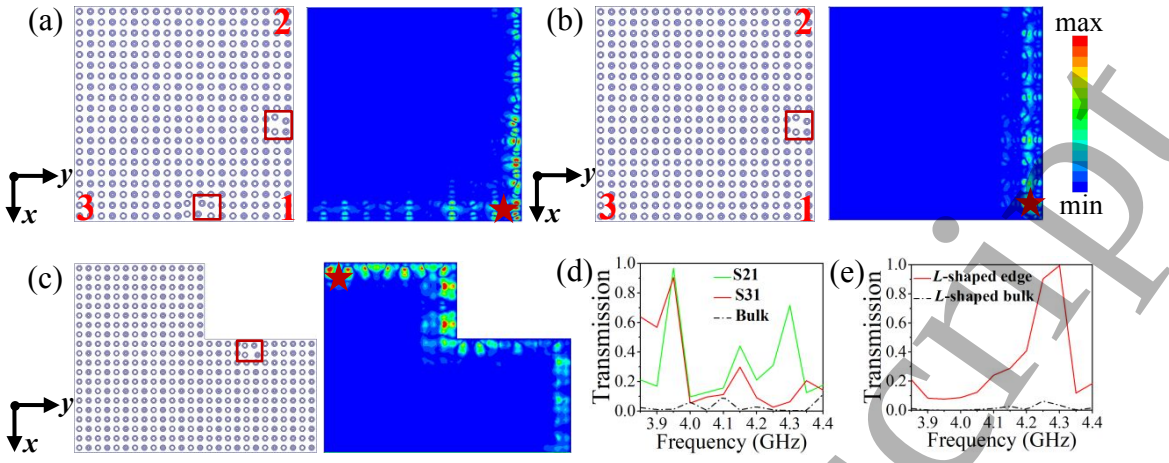

Figure 9. Position perturbations are introduced in the waveguide structure. The red boxes represent the location of the position perturbation. Electric field distribution of the 2D waveguide at the (a) 3.95 GHz and (b) 4.29 GHz by introducing a position perturbation. (c) 2D *L*-shaped waveguide structure by introducing a position perturbation at 4.29 GHz. (d) Transmission spectrums of the 2D square-waveguide by introducing a position perturbation. (e) Transmission spectrums of *L*-shaped structure by introducing a position perturbation.

4.2 Waveguide consisting of chiral subarrays with opposite chirality

It has been proved that the waveguide composed of CCW chiral subarrays can achieve robust transmission. In this section, as shown in Figure 10(a), we construct a waveguide composed of CW and CCW chiral subarrays, effectively forming an interface. The left sides of the black dotted rectangle are CW chiral subarrays, and the right sides of the black dotted rectangle are CCW chiral subarrays. The electric field distribution shows that the electromagnetic waves can propagate along the interface without obvious diffusion and backscattering.

Position disorder and frequency disorder are introduced at the interface to verify the propagation robustness. The simulated electric field distributions are shown in Figures 10(b) and 10(c), where the red boxes indicate the location of the disturbance. It can be seen that the electromagnetic waves can still propagate along the interface for the two kinds of perturbations. The transmission spectrums shown in Figure 10(d), which are in agreement with the simulated electric field distributions.

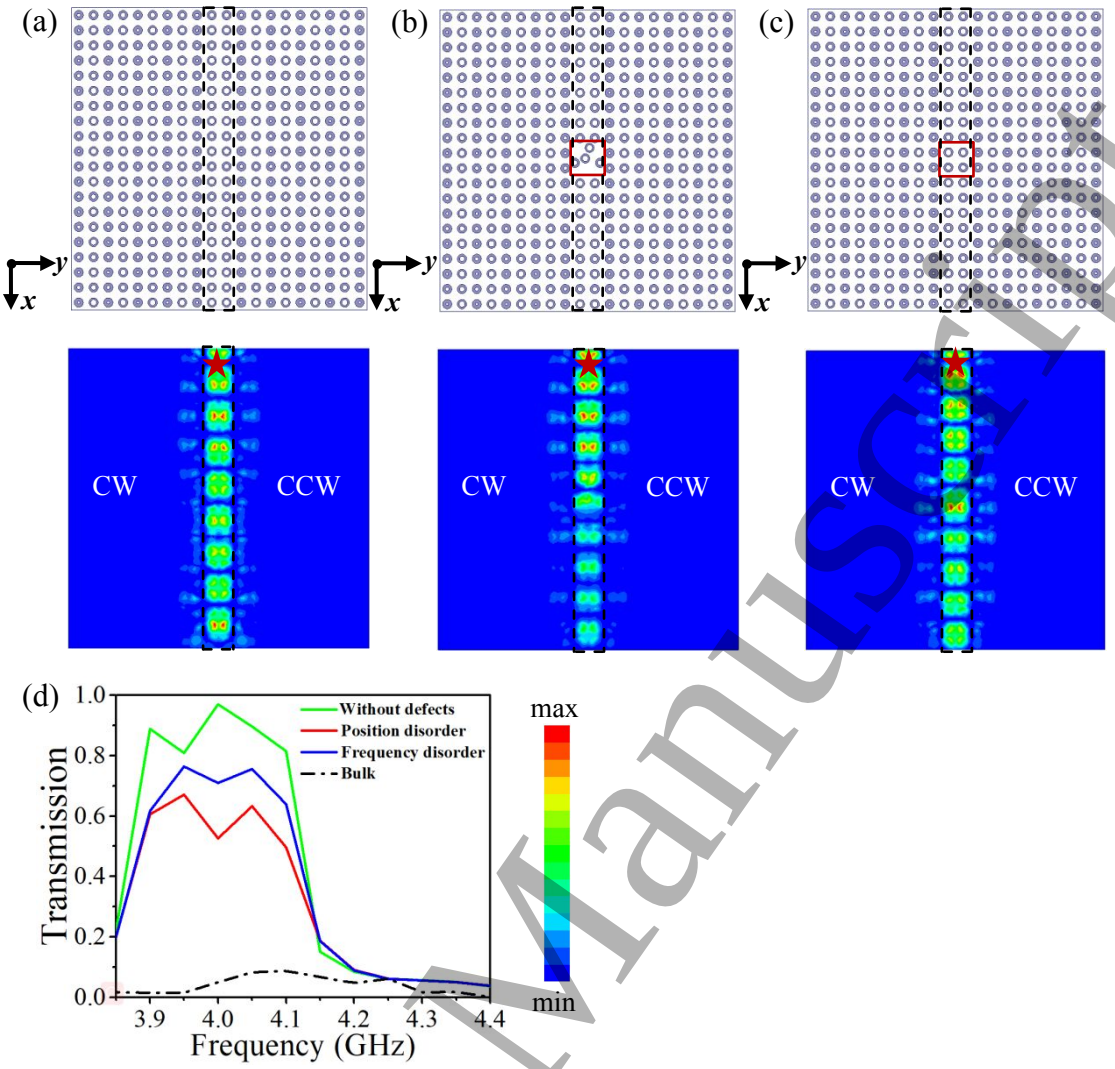

Figure 10. Waveguides and corresponding electric field distributions composed of the opposite chirality subarrays. (a) Electric field distribution at 3.95 GHz without defects. Electric field distributions at 3.95 GHz when introducing a (b) position disorder and (c) frequency disorder. (d) Transmission spectrums of the waveguide composed of CW and CCW chiral subarrays.

5 Applications

5.1 Duplexer

A novel duplexer operated at 3.94 GHz and 4.28 GHz is proposed, consisting of CCW chiral subarrays. There are 20 chiral subarrays along the *x* direction and *y* direction respectively. Figure 11 shows the electric field distributions at 3.94 GHz and 4.28 GHz. At the frequency of 3.94 GHz, the electromagnetic waves can transmit upward, whereas the electromagnetic waves propagate in the opposite direction at 4.28 GHz. Due to the edge states, there is no backscattering even if there is a sharp angle in the transmission interface.

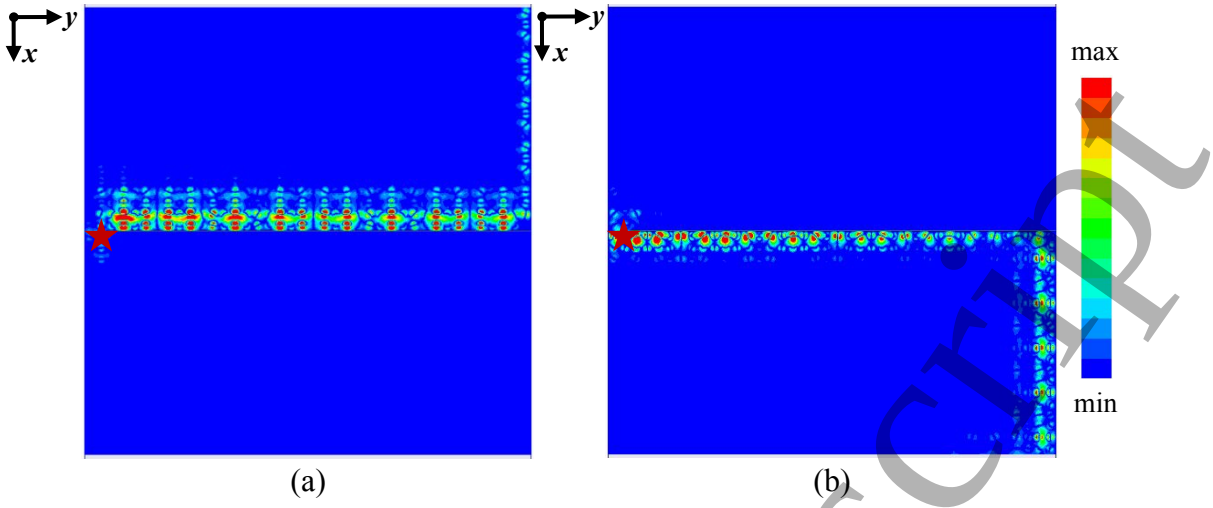

Figure 11. Electric field distributions of the duplexer at (a) 3.94 GHz and (b) 4.28 GHz.

5.2 Power divider

In this section, we construct building blocks by using the proposed chiral subarrays to realize a power divider. A three-way power divider is constructed by using the present chiral subarrays. The power divider can be easily obtained by increasing the number of chiral subarrays. Five CCW chiral subarrays are arranged into a 1D chain along the *x* direction, 2D case can be obtained by repeating the 1D chain 16 times along the *y* direction. Figure 12(a) shows the diagram of the three-way power divider, which presents PEC boundary condition (the green rectangle) is set every 5 CCW chiral subarrays along the *y* direction. The three-way power divider shown in Figure 12(a) is formed by repeating a 1D chain along the *y* direction (*x* direction), and the 1D chain is formed by a CCW chiral subarray along the *x* direction (*y* direction). Therefore, combined with the edge modes shown in Figures 3(b) and 4(b), there is an edge state in the three-way power divider interface at 4.29 GHz. Figure 12(b) presents the simulated electric field distribution, which shows that the electromagnetic waves can transmit in the expected three directions.

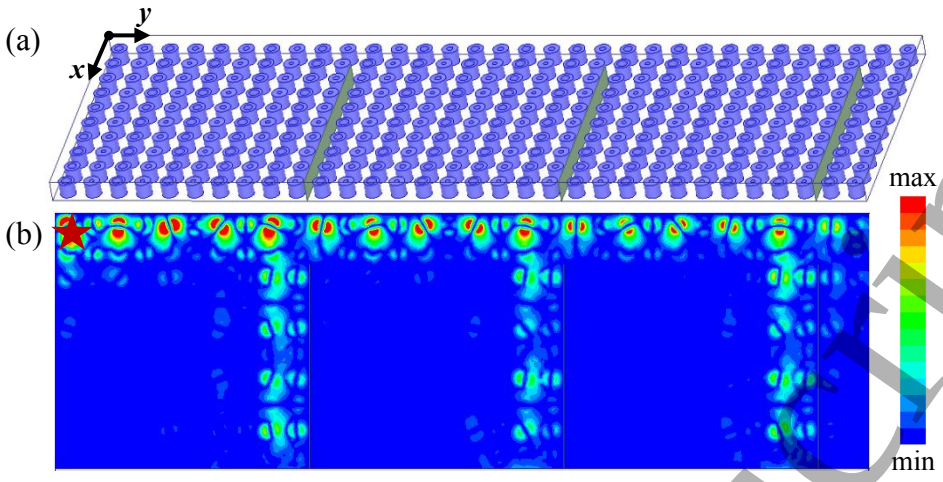

Figure 12. (a) Diagram of the three-way power divider. (b) Electric field distributions of the three-way power divider at the frequency of 4.29 GHz.

6 Conclusions

In conclusion, an all-dielectric dual-band chiral photonic crystal which can guide the robust transmission of electromagnetic waves is demonstrated. The elementary building block of the all-dielectric chiral photonic crystal is chiral subarray (CCW and CW chiral subarray), which can achieve two chirality corresponding the two types of edge states. We construct waveguides by using the chiral subarrays, where the electromagnetic waves can transmit in the waveguides without backscattering, and the transmission is immune to the position disorder and frequency disorder. Finally, a duplexer and a power divider are designed by using the present chiral photonic crystal. It is expected that the microwave devices implemented by the chiral photonic crystal could be an attractive candidate for communication systems.

Conflict of Interest

The authors declare that they have no competing interests.

Author Contributions

Y. L. conceived the idea and supervised the project. L. D., L. T., M. L., and X. Z. performed the numerical simulations. K. S., R. J., and X. Z. did the theoretical analysis. All authors contributed to the discussion. L. D, Y. L., and M. N.-C. co-wrote the manuscript.

Acknowledgments

Y. L. acknowledges support from the National Natural Science Foundation of China (Grant No.11874301), and the Natural Science Basic Research Plan in Shaanxi Province of China (Grant No. 2020JM-094). R. J. acknowledges support from the National Natural Science Foundation of China (Grant No. 61805204). K. S. acknowledges support from the National Natural Science Foundation of China (Grant No. 61601375), M. N.-C acknowledges support from the University of Birmingham (Birmingham Fellowship) and the European Union's Horizon 2020 research and innovation program (Grant No. 777714).

References

[1] Klitzing K V, Dorda G and Pepper M 1980 *Phys. Rev. Lett.* 45 494

[2] Thouless D J, Kohmoto M, Nightingale M P and Nijs M D 1982 *Phys. Rev. Lett.* 49 405

[3] Haldane F D M 1988 *Phys. Rev. Lett.* 61 2015-18

[4] Vonklitzing K 1986 *Rev. Mod. Phys.* 58 519-31

[5] Hasan M Z and Kane C L 2010 *Rev. Mod. Phys.* 82 3045-67

[6] Qi X L and Zhang S C 2011 *Rev. Mod. Phys.* 83 1057-110

[7] Bernevig B A, Hughes T L and Zhang S C 2006 *Science* 314 1757

[8] Lu L, Joannopoulos J D and Soljačić M 2014 *Nat. Photonics* 8 821-29

[9] Chen B G, Upadhyaya N and Vitelli V 2014 *Proc. Natl. Acad. Sci. U. S. A.* 111 13004-9

[10] Paulose J, Chen B G and Vitelli V 2015 *Nat. Phys.* 11 153-6

[11] Meeussen A S, Paulose J and Vitelli V 2016 *Phys. Rev. X* 6 041029

[12] Nash L M, Kleckner D, Read A, Vitelli V and Turner A M 2015 *Proc. Natl. Acad. Sci. U. S. A.* 112 14495-500

[13] Susstrunk R and Huber S D 2015 *Science* 349 47-50

[14] Vila J, Pal R K and Ruzzene M 2017 *Phys. Rev. B* 96 134307

[15] Xiao M, Ma G, Yang Z, Sheng P, Zhang Z Q and Chan C T 2015 *Nat. Phys.* 11 240-4

[16] Khanikaev A B, Fleury R, Mousavi S H and Alu A 2015 *Nat. Commun.* 6 8260

[17] Mousavi S H, Khanikaev A B and Wang Z 2015 *Nat. Commun.* 6 8682

[18] Fleury R, Khanikaev A B and Alu A 2016 *Nat. Commun.* 7 11744

[19] He C, Ni X, Ge H, Sun X C, Chen Y B, Lu M H, Liu X P and Chen Y F 2016 *Nat. Phys.* 12 1124-29

[20]Peng Y G, Qin C Z, Zhao D G, Shen Y X, Xu X Y, Bao M, Jia H and Zhu X F 2016 *Nat. Commun.* 7 13368

[21]Liu T W and Semperlotti F 2018 *Phys. Rev. Appl.* 9 014001

[22]Geng Z G, Peng Y G, Li P Q, Shen Y X, Zhao D G and Zhu X F 2019 *J. Phys.-Condes. Matter* 31 245403

[23]Ozawa T, Price H M, Amo A, Goldman N and Carusotto I 2019 *Rev. Mod. Phys.* 91 015006

[24]Lu L, Joannopoulos J D and Soljačić M 2016 *Nat. Phys.* 12 626

[25]Bahari B, Nado A, Vallini F, El A A, Fainman Y and Kante B 2017 *Science* 358 636-40

[26]Li M Y, Sinev I, Benimetskiy F, Ivanova T, Khestanova E, Kiriushechkina S, Vakulenko A, Guddala S, Skolnick M, Menon V M, Krizhanovskii D, Alu A, Samusev A and Khanikaev A B 2021 *Nat. Commun.* 12 4425

[27]Guddala S, Komissarenko F, Kiriushechkina S, Vakulenko A, Li M, Menon V M, Alu A and Khanikaev A B 2021 *Science* 374 6564

[28]Dikopoltsev A, Harder T H, Lustig E, Egorov O A, Beierlein J, Wolf A, Lumer Y, Emmerling M, Schneider C, Hofling S, Segev M and Klembt S 2021 *Science* 373 6562

[29]Liu S, Ma S J, Shao R W, Zhang L, Yang B, Navarro-Cia M, Cui T J and Zhang S 2021 *New J. Phys.* 23 103005

[30]Harari G, Bandres M A, Lumer Y, Rechtsman M C, Chong Y D, Khajavikhan M, Christodoulides D N and Segev M 2018 *Science* 359 1230

[31]Bandres M A, Wittek S, Harari G, Parto M, Ren J, Segev M, Christodoulides D N and Khajavikhan M 2018 *Science* 359 1231

[32]Lustig E, Weimann S, Plotnik Y, Lumer Y, Bandres M A, Szameit A and Segev M 2019 *Nature* 567 356

[33]Yang Y, Gao Z, Xue H, Zhang L, He M, Yang Z, Singh R, Chong Y, Zhang B and Chen H 2019 *Nature* 565 622

[34]Xie B Y, Wang H F, Wang H X, Zhu X Y, Jiang J H, Lu M H and Chen Y F 2018 *Phys. Rev. B* 98 205147

[35]Wang D Y, Yang B, Gao W L, Jia H W, Yang Q L, Chen X Y, Wei M G, Liu C X, Navarro-Cia M, Han J G, Zhang W L and Zhang S 2019 *Nat. Phys.* 15 1150-55

[36]Haldane F D M and Raghu S 2008 *Phys. Rev. Lett.* 100 013904

[37]Raghu S and Haldane F D M 2008 *Phys. Rev. A* 78 033834

[38]Wang Z, Chong Y D, Joannopoulos J D and Soljačić M 2008 *Phys. Rev. Lett.* 100 013905

[39]Wang Z, Chong Y D, Joannopoulos J D and Soljačić M 2009 *Nature* 461 772-5

[40]Yin P, Wu R X, Lin Z F, Yang Y and Chan C T 2011 *Phys. Rev. Lett.* 106 093903

[41]Yang Y T, Xu Y F, Xu T, Wang H X, Jiang J H, Hu X and Hang Z H 2018 *Phys. Rev. Lett.* 120 217401

[42]Gao Y F, He L, Jiang Z, Sun J P and Ma Q L 2020 *Photonic Netw. Commun.* 39 135-42

[43]Gao Y F, Jiang Z, Liu K Y, Ma Q L, Sun J P, Song H and Zamani M 2020 *J. Phys. D-Appl. Phys.* 53 365104

[44]Huang H B, Huo S Y and Chen J J 2019 *Crystals* 9 221

[45]Goryachev M and Tobar M E 2016 *Phys. Rev. Appl.* 6 064006

[46]Vázquez-Lozano J E and Martínez A 2018 *Phys. Rev. Lett.* 121 043901

[47]Alpeggiani F, Bliokh K Y, Nori F and Kuipers L 2018 *Phys. Rev. Lett.* 120 243605

[48]Geng Z G, Peng Y G, Shen Y X, Zhao D G and Zhu X F 2019 *Acta Phys. Sin.* 68 227802

[49]Orazbayev B, Kaina N and Fleury R 2018 *Phys. Rev. Appl.* 10 054069

[50]Ezaki K, Baba Y, Takahashi H, Shibata K and Nakano S 1993 *Jpn. J Appl. Phys.* 32 4319-22

[51]Liu C X, Rybin M V, Mao P, Zhang S and Kivshar Y 2019 *Phys. Rev. Lett.* 123 163901